



Fluid migration in continental subduction: The Northern Apennines case study

Nicola Piana Agostinetti*, Irene Bianchi, Alessandro Amato, Claudio Chiarabba

Istituto Nazionale di Geofisica e Vulcanologia, Centro Nazionale Terremoti, Via Vigna Murata 605, 00143, Rome, Italy

ARTICLE INFO

Article history:

Received 26 May 2010

Received in revised form 20 October 2010

Accepted 31 October 2010

Available online 20 January 2011

Editor: L. Stixrude

Keywords:

fluid migration

seismic anisotropy

Northern Apennines

receiver function

ABSTRACT

Subduction zones are the place in the world where fluids are transported from the foredeep to the mantle and back-to-the-surface in the back-arc. The subduction of an oceanic plate implies the transportation of the oceanic crust to depth and its metamorphization. Oceanic sediments release water in the (relatively) shallower part of the subduction zone, while dehydration of the subducted basaltic crust allows fluid circulation at larger depths. While the water budget in oceanic subduction has been deeply investigated, less attention has been given to the fluids implied in the subduction of a continental margin (i.e. in continental subduction). In this study, we use teleseismic receiver function (RF) analysis to image the process of water migration at depth, from the subducting plate to the mantle wedge, under the Northern Apennines (NAP, Italy). Harmonic decomposition of the RF data-set is used to constrain both isotropic and anisotropic structures. Isotropic structures highlight the subduction of the Adriatic lower crust under the NAP orogens, from 35–40 km to 65 km depth, as a dipping low S -velocity layer. Anisotropic structures indicate the presence of a broad anisotropic zone (anisotropy as high as 7%). This zone develops in the subducted Adriatic lower crust and mantle wedge, between 45 and 65 km depth, directly beneath the orogens and the more recent back-arc extensional basin. The anisotropy is related to the metamorphism of the Adriatic lower crust (gabbro to blueschists) and its consequent eclogitization (blueschists to eclogite). The second metamorphic phase releases water directly in the mantle wedge, hydrating the back-arc upper mantle. The fluid migration process imaged in this study below the northern Apennines could be a proxy for understanding other regions of ongoing continental subduction.

© 2010 Elsevier B.V. All rights reserved.

1. Introduction

Water and hydrous minerals are key components of many geodynamic processes in subduction zones, from the genesis of earthquakes and episodic tremors at shallow depth (Abers et al., 2009) to the generation of melts and upwelling diapirs under the magmatic arcs (Stern, 2002). At greater depth, topography of the mantle transition zone has been linked to the water flow induced by the subduction of oceanic crust (Tonegawa et al., 2008). A widely accepted model for water transportation into the mantle, due to the subduction of oceanic lithosphere, considers: (1) fluids released from sediments, at shallow depth; and (2) the dehydration of subducting oceanic crust at 70–100 km depth (Hacker et al., 2003). Deeper water transportation implies the presence of a supra-slab serpentinized mantle dragged down within the descending slab (Iwamori, 1998). Continental subduction is likely to show a different behaviour, due to the intrinsic differences in the subducted materials and their response to subduction process. Due to its buoyancy, the continental lithosphere does not easily

sink in the upper mantle, generating gravitational instability which does not evolve as in oceanic subduction. Moreover, slices of continental crust can be dragged down coupled to the continental lithosphere inducing peculiar metamorphism (Whitney et al., 2010).

Many seismological observations have been used to catch the presence of water and hydrous minerals at depth, as well as the process of dehydration and water release. Anomalous high V_p/V_s ratio has been associated to water confined in the subducted, overpressured oceanic crust where the interface between the two plates is sealed at shallow depth (Audet et al., 2009). A seismological signature of water transportation in the fore-arc mantle is the presence of low S -wave velocity anomalies at depth, sub-parallel to the descending oceanic lithosphere, indicating the serpentinization of the supra-slab mantle (Kawakatsu and Watada, 2007) and water released from the dehydration of the oceanic mantle lithosphere. The upper planes of double Benioff Zones have been associated to dehydration reactions within the subducting oceanic crust (Brudzinski et al., 2007). Tomographic studies image rock mineral transformation into the descending crust as a variation of its seismic velocities with depth (Reyners et al., 2006). Seismic anisotropy is a less used marker for the presence of hydrated materials and fluids at depth, even if anisotropic materials are likely in a subduction zone. Serpentinization of the mantle wedge produces a zone of negative anisotropy (i.e. where the seismic velocity along the symmetry axis is lower than along the normal plane) on top of the slab (Park et al., 2004).

* Corresponding author.

E-mail addresses: nicola.piana@ingv.it (N.P. Agostinetti), irene.bianchi@ingv.it (I. Bianchi), alessandro.amato@ingv.it (A. Amato), claudio.chiarabba@ingv.it (C. Chiarabba).

Water released from the slab can induce partial melting of the mantle wedge peridotite, which displays strong anisotropic pattern (Takei, 2010). Finally, high pressure, hydrous metamorphic facies are intrinsic anisotropic, i.e. amphiboles (Christensen and Mooney, 1995).

1.1. Tectonic setting

Geodynamics of the Mediterranean area is mainly driven by the convergence between the Nubia and Eurasia plates, occurred in the last 100 million years (Faccenna et al., 2001). Due to this ongoing process, from the Upper Cretaceous the central Mediterranean was re-organised as micro-plates which accommodate the convergence in peculiar ways. One example is represented by the Apennines orogen, which strikes almost parallel to the convergence direction between the main Africa and Eurasia plates (Dewey et al., 1989). Furthermore, tomographic images of the upper mantle beneath the Apennines reveal the presence of a cold dipping body and its clear segmentation (Lucente et al., 1999), pointing out the complexity of this re-organisation process. A widely accepted hypothesis suggests that the oceanic domain which separated the two continents was progressively subducted under the Iberian–European margin due to slab pull, inducing trench retreat (Faccenna et al., 2001). Trench retreat has been observed elsewhere in the central Mediterranean region, and indicate a “path” of counterclockwise rotation of the subduction zone (Carminati et al., 1998). The process of slab retreat has been also invoked to explain the synchronous presence of coupled extension and compression along the subduction zone (Malinverno and Ryan, 1986; Mariucci et al., 1999), which is a long-standing observation in central Mediterranean (Frepoli and Amato, 1997). In the Apennines, starting 30 My ago, continental materials were incorporated in the orogenic wedge, following the

entrance of the continental margin of the Adria microplate at the trench, and leading to subduction of the continental lithosphere (Di Stefano et al., 2009; Faccenna et al., 2001). According to some authors (e.g. Channell and Mareschall, 1989) the Apennines continental subduction has evolved to a stage of “delamination” in which the continental lithosphere is detached by (part of) the crust and sinks in the upper mantle dragged by the oceanic lithosphere negative buoyancy (also called “post-subduction” delamination).

The Northern Apennines (NAP) is the portion of the belt comprised between 43° and 45° latitude (Fig. 1). In this region the strike of the chain rotate from WNW–ESE to N–S, giving to the orogens its arcuate shape. The NAP separates the Tuscan (West) from the Adriatic (East) regions. The two regions display very different characteristics: local seismicity (De Luca et al., 2009), rheology (Pauselli et al., 2010), crustal structure (Finetti, 2005), heat flux (Pauselli and Federico, 2002), geothermal fluids (Minissale et al., 2000) and stress field (Montone et al., 2004; Pondrelli et al., 2006). Tomographic studies highlighted the presence of a cold dipping body beneath the NAP chain and the Tuscan domain (Lucente et al., 1999). Such body has been interpreted as the cold oceanic lithosphere subducted under the Eurasia plate. Subcrustal seismicity is present beneath the Tuscan side of the orogens (De Luca et al., 2009), revealing the presence of a dehydrating body sinking into the upper mantle (Chiarabba et al., 2009) and confirming the subduction hypothesis.

1.2. Previous RF studies across Northern Apennines

Receiver functions (RF) are time-series which emphasise the *P*-to-*s* (*P*_s) converted waves in the *P* coda of teleseismic records. RF are computed through the deconvolution of the vertical from the horizontal

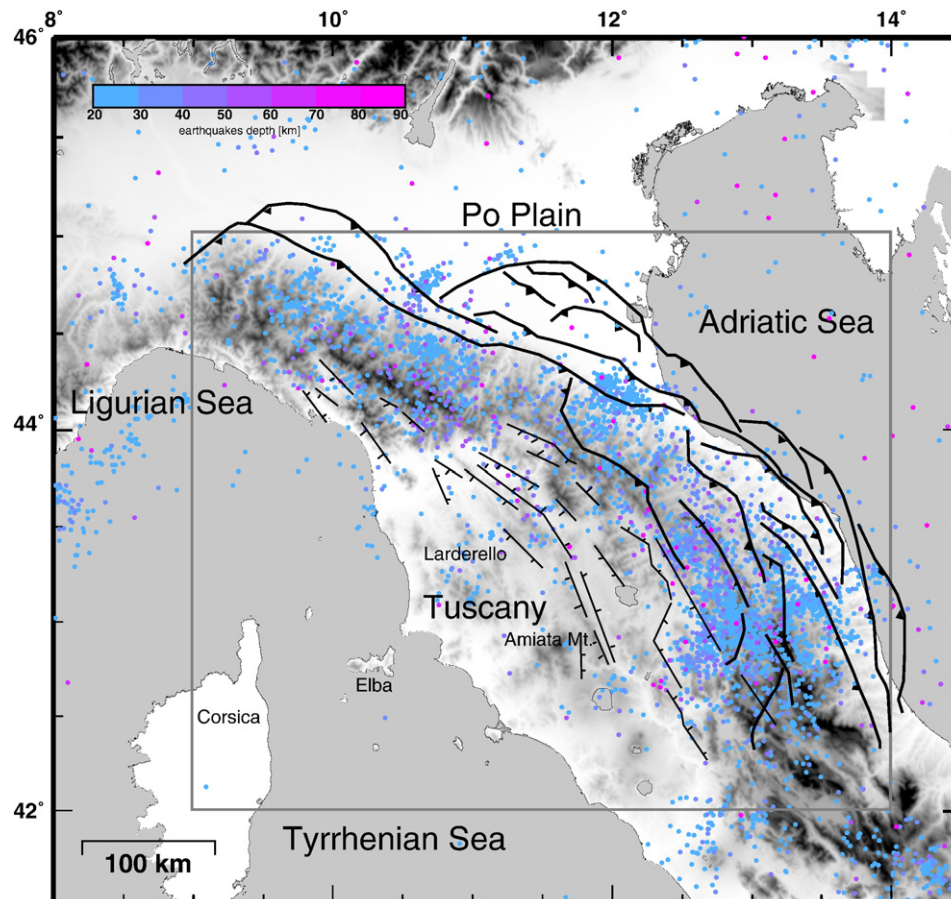


Fig. 1. Tectonic sketch of the study area. The curved black lines toward the Adriatic Sea are the traces of the more external thrust fronts. The thin black lines in the Apennines are the normal faults. Circles are epicenters of $Z > 35$ km seismicity. The rectangle depicts the area of the next figure.

seismograms. The amplitudes and time-delays of the arrivals recorded in the RF contain information about the buried seismic discontinuities beneath the receiver seismic station (Langston, 1979). Isotropic and anisotropic structures can be retrieved from the analysis of the RF as a function of the back-azimuth (Baz) of the incoming teleseismic wave (Savage, 1998). Simple 3D structures, like dipping interfaces and layers containing hexagonally anisotropic materials, generate periodic patterns in the RF data-set, as a function of Baz (Levin and Park, 1998). The analysis of such periodicity has been used to infer the presence of anisotropy in the subsurface (e.g. Bianchi et al., 2008) or dipping interfaces (e.g. Lucente et al., 2005). In a recent paper, Bianchi et al. (2010) applied an harmonic decomposition technique, which is suited to extract the information about the periodicity of the RF signal, to a linear deployment of seismic stations, producing images of the harmonic components at depth.

RF have been used to infer the bulk seismic velocity structures across many subduction zones (e.g. Abers et al., 2009; Bannister et al., 2004; Kawakatsu and Watada, 2007). However, few studies report the analysis of the off-plane energy (i.e. the Transverse component of the RF data-set) to better define such structures (e.g. Mercier et al., 2008; Savage et al., 2007; Tibi et al., 2008; Tonegawa et al., 2008). More, the analysis of the periodicity of the RF data-set for stations deployed across subduction zones is limited to Japan (Shiomi and Park, 2008) and Southern Italy (Piana Agostinetti et al., 2008b). In those cases, the local dip angle of the top of the subduction plate and the anisotropic behaviour of the mantle wedge have been studied, respectively.

The crustal structure across the NAP orogen has been investigated using RF in a number of studies (Piana Agostinetti and Amato, 2009, and references therein). Previous works were targeted only to the

isotropic structure of the crust and upper mantle. Thus, they exploited only the radial component of the RF data-set. RF studies confirm the presence of a thin 20-km thick crust along the Tuscan region (i.e. a shallow Tyrrhenian Moho). This seismic discontinuity is almost flat and can be traced from the coast to the orogen. On the other side, the Adriatic Moho is much more elusive and its depth is debated, ranging from 30 to 45 km depth. In any case, the Adriatic crust results, at least, 10 km thicker than the Tuscan crust. Under the Apennines, a double Moho has been inferred (i.e. Tuscan over Adriatic), but the data suggest the presence of more than one dipping seismic discontinuity at depth (Piana Agostinetti and Amato, 2009). Few recent studies were aimed to the detection of anisotropy in the crust and upper mantle in the NAP region (e.g. Roselli et al., 2010).

In this paper, we present a new analysis of RF which points out the presence of strong heterogeneities across the NAP chain, both in terms of isotropic and anisotropic properties of the crust and upper mantle materials. First, we review the previous work on crustal structure across the NAP chain. Then, we compute the harmonics decomposition of the RF data-set and we analyse the patterns of the *P*-to-*s* converted phase across the NAP orogen. Thus, we inverted the RF data-set, using a classical stochastic method, to constrain both the bulk seismic velocity and the anisotropic properties in the crust and upper mantle. Our results allow us to draw a detailed picture of the NAP subduction zone, which improve previous knowledge in the area. Following the alteration of the seismic properties of the incoming Adria plate from the Adriatic toward the Tyrrhenian sea, we infer new details of the migration of the fluids from the subducting plate to the Apenninic wedge.

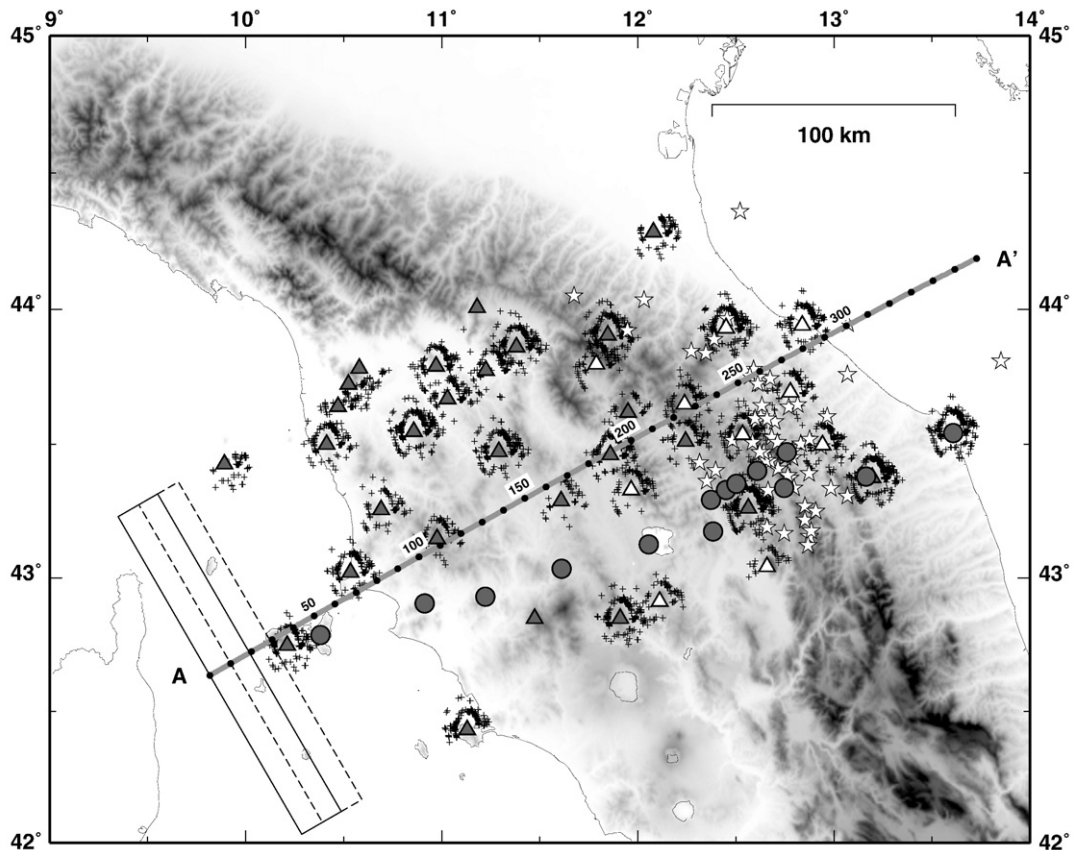


Fig. 2. Map showing seismic site locations and ray piercing-points at 40 km depth (crosses). Triangles represent stations used to compute the RF shown in Figure 4. Circles indicate temporary stations used in previous works for Moho depth estimates. Stations marked with unfilled symbols have no Moho depth estimates. White stars are local earthquakes with focal depth greater than 35 km. A grey line indicates the vertical profile AA' trace, and black dots show the locations of the spots used to compute RF in Figure 4. Distance along the profile is also reported for reference. Boxes at the beginning of the profile show the overlapping scheme used to compute RF in Figure 4.

2. Data and methods

2.1. Data processing for RF harmonic decomposition

In this study, we analyse teleseismic records from both temporary and permanent broadband seismic stations (Fig. 2) deployed across the northern part of the Italian peninsula, from the Tyrrhenian to the Adriatic coast. Here, we briefly review the data selection and analysis.

Teleseisms are selected based on their magnitude ($M_w > 5.5$) and epicentral distance (Δ , $30 < \Delta < 100$). After a first visual inspection, through which we exclude seismic waveforms with a low s/n ratio, we obtain a data-set of about 15,000 3-component records, with a minimum of 120 and a maximum of 670 records for each station. We rotate teleseismic records in the LQT system, where L is the theoretical direction of the incoming P -wave-field, Q is computed along the great circle path from the source to the station and normal to Q , and T is the normal to the QL plane, positive 90° CW from L . Then, we computed the RF data-set using the multitaper correlation code developed by Park and Levin (2000), with a cut-off frequency of 0.5 Hz. To highlight the main variation of the seismic structure under the NAP chain, the RF data-set is projected along a $N60^\circ$ profile which is locally normal to the strike of the orogen. We filter our RF data-set using a box-shaped moving window of 10 km half-width, 50% overlapping scheme and we obtain an ensemble of evenly spaced “spots” of RF. For each spot, both radial (Q) and transverse (T) components, are analysed in terms of their periodicity as a function of the incoming P -wave back-azimuth (Baz). This analysis consists of a decomposition of the P -to- s converted wave-field in five terms. A first term represents the P -to- s converted energy from isotropic velocity jumps, which is independent from the back-azimuth of the incoming wave-field. Two terms contain the converted energy which displays a 2π periodicity with Baz, for two normal directions (i.e. N–S and E–W), while the last two terms display the variability of the RF with a π periodicity along two normal directions. We refer to Bianchi et al. (2010) for a detailed description of the decomposition method. Here, we summarise the importance of such decomposition. For a horizontal seismic discontinuity between two isotropic media, the P -to- s converted energy will be displayed only on the first term, while the other four terms should be zero. For a dipping discontinuity, or for a horizontal discontinuity between anisotropic media with plunging symmetry axis, the energy will be mainly distributed between the first three terms. Finally, for a horizontal discontinuity between anisotropic media with horizontal symmetry axis, the energy will be found in the first term and in the last two (see Bianchi et al. (2010, Fig. S1) for detailed examples). As clearly reported in Bianchi et al. (2010), the analysis of the decomposition of the RF data-set allows to separate effects due to different heterogeneities, giving a fundamental support to the interpretation of a RF data-set in complex geodynamic settings like the Northern Apennines. Here we follow Bianchi et al. (2010) and we focus our data-set on the 20–70 km depth range, where we expect that the Apennines wedge develops. This depth range fills a gap between local earthquakes and teleseismic tomography, unravelling peculiar details of the seismic structures which could elude other kinds of seismic investigations.

2.2. RF inversion

To extract precise information on the seismic properties at depth, we apply a classical stochastic method to invert our decomposed RF data-set. We follow the approach developed in Sambridge (1999) and we implemented a global search in the parameter space, from which we obtain an ensemble of good data-fitting models. (R1.6) Here, we briefly outline the main steps of this method. Our parametrisation comprises both dipping planar interfaces and anisotropic layers. Forward modeling is achieved using the method presented in Frederiksen and Bostock (2000). (R2.4) For each spot, forward

modelling is computed using the back-azimuth and the slowness of the RF in the observed data-set. Following Bianchi et al. (2010), we divide the profile in three areas, adopting a peculiar parametrisation for each region. Then, we follow a two step approach. First, the classical Neighbourhood Algorithm inversion is applied (as in Bianchi et al., 2008) to retrieve the bulk properties for each single spot of our data-set. Both isotropic and anisotropic (if present) properties are investigated at the same time and a single best-fit model is individuated for each spot. (R1.6) Second, for each different region, the seismic velocities of the different subsurface structures (i.e. the crust, the mantle wedge the subducted Adriatic crust and the upper mantle) retrieved in best-fit models are averaged. At this point, we perform a second run of the Neighbourhood Algorithm inversion using the mean seismic values obtained from the first inversion and searching for the depth of the interfaces and the anisotropic parameters of the buried body. (R1.6) Formal errors on the inverted parameters are estimated from the best-fit family of sampled models. Best-fit family comprises models which obtained a fit less than 1.2 times the best-fit model fit. For the elastic parameters, we computed errors from the best-fit families obtained during the first step of the inversion, while for the depths of the interfaces and the anisotropy parameters, errors are evaluated from the best-fit families of the second inversion step. For each parameter, minimum and maximum values are extracted from the best-fit family and the half-width of their difference is used as error estimate. For the depth parameters, we find that a conservative value for the uncertainty is ± 5 km, even if we observe an increase of the uncertainties for the deeper interfaces. We associate a ± 0.2 km/s uncertainty to the S -velocity parameters. The error on V_p/V_s ratio is estimated as large as ± 0.03 . Anisotropic percentage and the axis direction angles are estimated with errors as large as $\pm 2\%$ and $\pm 5^\circ$, respectively.

3. Results

3.1. Review of previous RF studies and local seismicity

We review in details all previous RF studies in the area to give a starting point to our analysis and to better define the previous knowledge about the seismic structure in this zone. Also, we compare these results to the most recent local earthquakes catalogue (De Luca et al., 2009) for the area, and we report the surface evidence of the main extensional and compressive faults along the profile to obtain a comprehensive image of different seismic studies. In Figure 3, we report all previous results for the Moho depth obtained using RF projected along the profile AA'. As expected, complexities arise under the mountain chain, from $X=200$ to $X=300$ km along the profile. We use different colours to define three different interfaces present at depth. Dashed lines indicate the linear fit to the coloured symbols. From the Tyrrhenian coast to the Val Tiberina (ATF in Fig. 3, $0 < X < 210$ km), the results indicate the presence of a shallow sub-horizontal S -velocity discontinuity (about 20–25 km depth), usually interpreted as the Tyrrhenian Moho. Under the highest portion of the orogens, there are two different, almost parallel, west-dipping interfaces, which can be traced from 30 to 50 km depth. Linear trends indicate a dip angle of 29° and 20° for the lower and upper interfaces, respectively. The former seems to shallow from 55 km depth, at $X=210$ km, to about 40 km depth, at $X=250$ km. The latter shallows from 50 km depth, at $X=250$ km, to about 30 km depth, at $X=290$ km. Results at the Adriatic coast, at about $X=320$ km, based all on the same small temporary data-set, seem controversial. However, Moho depth ranges between 30 and 45 km depth.

RF results are compared with the more recent local earthquake catalogue by (De Luca et al., 2009). Events were selected using three consecutive selection criteria. Events were discarded if: (1) they were located with less than 10 phases; (2) their location errors were larger than 1 km (both vertical and horizontal); and finally, (3) their RMS

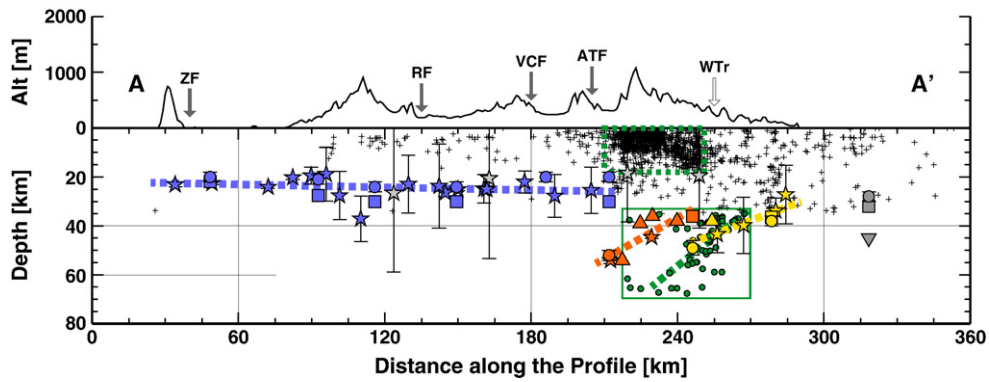


Fig. 3. Review of previous results on Moho depth in the study area and local seismicity. Symbols indicate different sources: circles, results from Mele and Sandvol (2003); squares – Piana Agostinetti et al. (2002); inverted triangles – Levin et al. (2002); triangles – Roselli et al. (2008); stars – Piana Agostinetti and Amato (2009). Symbol colours illustrate the different interfaces found and dashed lines represent linear interpolation of the symbols. Grey stars are stations with large 1σ errors in Moho depth, not included in the linear interpolations. Crosses and green filled circles indicate shallow and deep local seismicity, respectively. Green dashed box delimits the area with high-density of shallow earthquakes. Green box delimits the area of occurrence of deep events. Seismicity is redrawn from De Luca et al. (2009)'s catalogue. Topography along the vertical profile is shown on top of the main panel. Grey arrows indicate normal faults: ZF – Zocale fault; RF – Radicondoli fault; VCF – Val di Chiana fault; ATF – alto Tiberina fault. An unfilled arrow marks the westernmost trust (fault positions from Collettini et al. (2006)).

was greater than 0.1. We obtain a sub-catalogue of about 4571 events. In Figure 3, crosses show the selected earthquakes, while green filled circles display deeper (>35 km focal depth) seismicity. Earthquake depths range from 0 to about 70 km depth and, from West to East, we clearly define the different characteristics of the seismicity. From the Tyrrhenian coast to about $X=200$ km, a low level of seismicity is confined in the upper crust. Shifting eastward, seismic activity strongly increases. From $X=210$ km to 250 km, a very high level of micro-seismicity (green dashed box in Fig. 3) is evident from the surface (at $X=210$ km) to about 20 km depth (at $X=240$ km). We notice that, in this portion of the profile, diffuse seismicity occurs also in the deeper portion of the crust (down to 30 km). At $X=250$ km the micro-seismicity level abruptly decreases. From here to the Adriatic coast, local earthquakes are homogeneously distributed over all the crustal volume. Deeper seismicity (green box in Fig. 3) is confined between $X=210$ km and $X=280$ km. The observed pattern clearly displays a trend that shallows from West to East. Shallower events seem to cluster along a West-dipping interface. Events with depth greater than 55 km seem more widely spread. We compute a linear interpolation (green dashed line) of the deeper seismicity, using a 50%-trimmed ensemble to down-weight the outliers. Estimated dip angle of the west-dipping seismicity is about 38° , close to the 40° proposed by (Selvaggi and Amato, 1992) on older data. We observe that the linear trend of the deeper seismicity cut the westernmost interface found by previous RF studies (yellow dashed line) in its deeper portion, at about 50 km depth.

3.2. Harmonic decomposition of the RF data-set

In Figure 4, we show the harmonic decomposition of the RF data-set projected along the profile AA'. The top panel (Fig. 4a) reports the Constant part, which mirrors the isotropic S -velocity structure. Anisotropic and/or dipping layer contributions are visible on the Cosine (N–S) and Sine (E–W) components, for 2π -periodicity, reported in Figure 4bc. The RF data-set has been sampled every 10 km using a box-shaped filter with 10 km half-width and migrated to 40 km depth. This projection scheme gives us an ensemble of wiggles distributed every 10 km with 50% overlapping zone between adjacent wiggles. The average number of teleseismic events which compose a wiggle is 552, with a minimum of 109 and a maximum of 1104. Roughly, the migration process correctly focuses the RF image between 10 and 70 km, so that a careful analysis of the three panels gives us a first-order description of the crust–mantle boundary and of the uppermost mantle wedge along the profile.

First, we observe the presence of energetic and coherent arrivals on the Constant part which reveal continuous first-order seismic discontinuities at depth (Fig. 4a). Positive (negative) isotropic seismic discontinuities at depth, i.e. where seismic velocities increase downward (upward), generate a signal on the Constant plot which is represented by a blue (red) wiggle. Three main positive arrivals are traceable along the profile. A first blue pulse is visible between 20 and 35 km depth from the Tyrrhenian coast to, at least, $X=200$ km where its amplitude vanishes. A second pulse is clearly seen at about 70 km depth ($X=180$ km) and raises up to 55 km depth ($X=220$ km). From the Adriatic side, a broad positive pulse at about 40 km depth ($X=320$ km) increases its depth under the orogens (80 km depth at $X=210$ km) defining a west-dipping interface. The three described pulses are marked in Figure 4 using a light blue, orange and yellow circles, respectively. Two red areas are also recognisable: a faint negative pulse between $X=190$ and $X=220$ km between 40 and 60 km depth; and a broad negative pulse along the Adriatic side at about 80 km depth. We observe that the two westernmost positive pulses (orange and yellow circles) terminated to the east in a broad positive area extending between 60 and 100 km depth. Here, our migration model does not correctly focus the energy, so that we prefer to exclude these pulses from the analysis.

Coherent patterns are also present in the plots of the Cosine and Sine components (Fig. 4bc). As previously stated, in these plots, both blue and red wiggles mark the presence of anisotropic and/or dipping discontinuities, and a combination of the two roughly indicates the symmetry direction of these features. On the Cosine component, positive (negative) arrivals indicate a North (South) direction. East (West) direction is represented by positive (negative) arrivals on the Sine Component. Colour code is the same as for the Constant part, i.e. blue is positive. At a first glance, stronger arrivals are present on the Cosine plot, which reflects a preferential N–S orientation of the structure, rather than E–W. In the following, we analyse in detail the Cosine plot, using the Sine plot only to constrain the symmetry directions in the following inversion. In Figure 4b, purple and pink filled circles denote main negative and positive arrivals, respectively. From the distribution of these pulses, we define a zone along the profile (marked with a purple box) where strong energy is decomposed in the first harmonics. West of this area, we identify a zone where 3D structure are almost absent, from $X=40$ to $X=170$ km. In this interval, very low energy is present both on the Cosine and Sine plots, suggesting a very simple seismic structure. From $X=180$ to $X=240$ km, the marked box, between 40 and 80 km depth, we observe a strong derivative pulse, i.e. a positive pulse

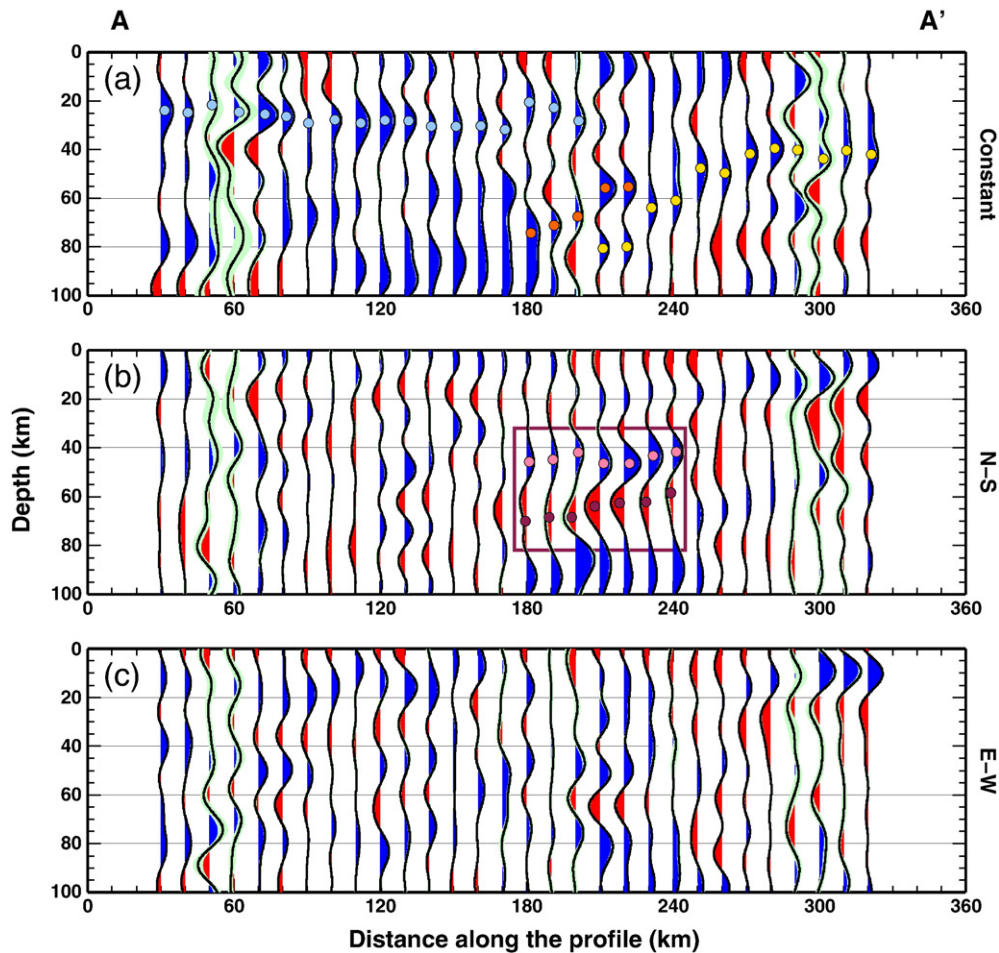


Fig. 4. Harmonic decomposition of the RF data-set. (a) “Constant” $k=0$ harmonics. Cyan, orange and yellow dots indicate the three main pulses analysed. (b) The N-S $\cos\phi$ term of the $k=1$ harmonics. A purple box delimitates the area where the two main pulses are present, indicated with pink and red dots. (c) The E-W $\sin\phi$ term of the $k=1$ harmonics.

followed by a negative pulse of similar amplitude. The presence of this pulse defines an area where later arrivals are almost absent. The pulse displays a gently west-dipping behaviour. However, its dip is clearly less pronounced than for the interfaces found in the Constant plot. (R2.5) The absence of a corresponding pulse in the Constant plot indicates that the origin of such energy in the Cosine plot needs to be related to an interface between isotropic and anisotropic materials which share the same mean V_s velocity. Also, this fact excludes the presence of a steeply dipping interface, which likely produces recognisable pulses on both the Constant and the Sine plots (due to the profile orientation, N60°E. The depth-distance between positive and negative pulses seems to increase toward W. Also, in this area coherent pulses are found in the Sine (E–W) plot (Fig. 4c), but far less evident. Last, in the eastern part of the profile, no coherent arrivals are found, even if small amplitude west-dipping phases can be observed in the Cosine plot. We observe that a broad positive pulse is present between $X=180$ and $X=240$ km, at about 90 km depth. As for the Constant part, we do not correctly focus this depth level, due to the migration model, and we prefer to exclude these pulses from the analysis.

Summing up, the analysis of the decomposed RF data-set, together with the review of the previous RF results obtained in the area and analysis of the local seismicity, suggests the division of the study area in five zones, which present different crustal and upper mantle properties. We illustrate this hypothesis in Figure 5, where we report all the observations highlighted earlier. At the first-order, we give the

following characterisation of the crust and upper mantle under the profile. Zone A is marked by a shallow and almost horizontal interface which defines the crust–mantle boundary. We find no evidence for an upper mantle stratification and local seismicity is almost absent. Zone B is defined by the presence of coherent energy on the first harmonics. This zone is subdivided in three different areas (marked with numbers in Fig. 5), due to the relative position of the pulses in the Constant and Cosine plot in Figure 4. In Zone B1, energy in the first harmonics is confined above the deepest pulse traced in the Constant plot, i.e., the origin of the periodic pulses resides above the isotropic interface. Zone B2 is characterised by the presence of energy in the Cosine plot both above and below the upper isotropic pulse defined in the Constant plot. The lowermost pulse in the Constant plot is deeper than both the periodic pulses. In Zone B3, periodic energy, recorded in the Cosine plot, is above the deepest interface of the Constant plot, but seems to be confined above by one of the interfaces defined in Figure 3, indicating that the origin of such energy is trapped between two dipping seismic discontinuities. Also, deep seismicity is only present in Zone B3, where it follows the dip of the lowermost interface. On the Adriatic side, Zone C displays a low-angle dipping interface on the Constant plot. Here, deep seismicity presents a steeper dip angle than the isotropic interface. Finally, shallow, dense local seismicity is confined in the portion of the orogens which sits above Zones B2 and B3.

A first interpretation of this analysis leads us to consider a division of the NA subduction system in three parts, as previously highlighted in

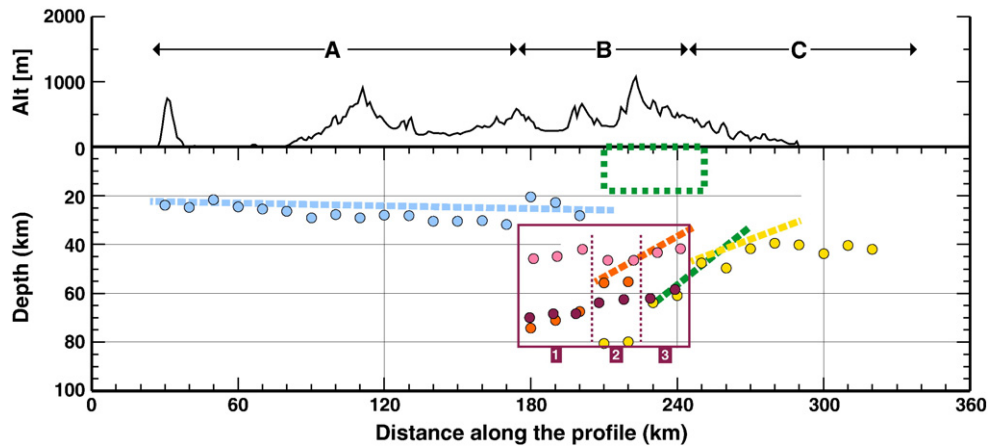


Fig. 5. Summary of the RF analysis. Cyan, orange and yellow dashed lines are taken from Figure 3 and represent the previous results about the Moho depth obtained in the study area using RF analysis. The green dashed line and the green dashed box indicate the linear trend of the deep seismicity and the dense shallow local seismicity, respectively. Coloured circles and the purple box from are taken Figure 4 and display the main pulses on both the “constant” $k=0$ and the $k=1$ harmonics. Letters mark the three different regions along the profile. Numbers indicate the three different zones where anisotropy develops. Topography is plotted on top, for reference.

Bianchi et al. (2010) for an adjacent portion of the orogens. From the Tyrrhenian sea toward the chain, our inferences on the seismic structure confirm the presence of a thin “Tyrrhenian” crust, 20–30 km thick, bounded by a sub-horizontal Moho discontinuity (Piana Agostinetti et al., 2008a) (our Zone A). From the Adriatic side toward the NAP, we identify a gently west-dipping Adriatic Moho, 40 km depth (Zone C). A thickness of about 30 km for the Adriatic crust has been estimated in the undeformed Puglia for-eland (Piana Agostinetti and Malinverno, 2010; Steckler et al., 2008). Heterogeneities in the Adria microplate (Finetti, 2005), and the presence of thick Pleistocene-to-Holocene fore-deep sediments (Patacca et al., 2008), might be responsible for our larger Moho depth. Zone B comprises the main portion of the orogens, from the westernmost thrust to the younger extensional basins (ATF and VCF, see Fig. 3). In this zone, our results highlight the presence of complex seismic structure at depth. As in Bianchi et al. (2010), the structure under the orogens displays both Tyrrhenian and Adriatic Mohos. The presence of strong periodic energy between the two interfaces is interpreted as the signature of an anisotropic zone, but our results highlight a different geometrical trend for the isotropic and anisotropic structures in this area. As described earlier, Zone B can be sub-divided in three sections, given the relative position of the isotropic and anisotropic pulses in Figure 4. Interpretation of the three sections requires a refined analysis of the seismic properties at depth, given in the next section. However, we observe that: (1) Zone B3 comprises a west-dipping anisotropic layer bounded by two isotropic jumps; (2) Zone B2 shows a complex anisotropic behaviour, as anisotropy is present in both the upper part of a deep west-dipping layer and in the lower part of the wedge above it; and (3) Zone B1 displays a single isotropic jump (other than the Tyrrhenian Moho at 25 km), coincident with the bottom of the anisotropic area, entirely developed in the wedge. As a whole, all these observations suggest that during the retreat of the Adriatic subduction zone (Malinverno and Ryan, 1986), part of the Adriatic lower crust is slowly subducted together with the Adriatic mantle lithosphere (Chiarabba et al., 2009; Di Stefano et al., 2009). (R1.2) This process is likely to induce a two-step metamorphism of the subducted crust. At shallow depth (where deeper seismicity is confined in the subducted crust) lower (granulitic or gabbroic) crust turns to blueschists with water release which triggers deeper seismicity. At larger depth, blueschists are eclogitized (Stern, 2002). The two metamorphic phases depend both on temperature and pressure. In Northern Apennines only Blueschists is at outcrops, but this does not exclude the formation of eclogite at depth, as eclogite can be negatively buoyant with respect to the surrounding mantle materials. Fluids released from the metamorphism of

the blueschists hydrate the mantle wedge triggering partial melts and/or serpentinization. The synchronous and progressive release of the fluids from the subducted lower crust and the retreat of the subducted plate give rise to a diffuse hydration of the Tyrrhenian mantle.

3.3. Inversion results

The analysis presented in Sections 3.1 and 3.2 defines a clear picture of the geometry of the subsurface structures, giving details for a qualitative interpretation of the results. As described in Section 2, a global inversion of the RF data-set is carried out to retrieve quantitative estimates of the seismic properties at depth, to verify the previous interpretations and give further details for the discussion. For each zone identified earlier (A, B1–3, and C), we define a parametrisation according to the observations made in Section 3.2 (see Table S1) for details). For the Tyrrhenian side (Zone A, from $X=0$ to $X=175$ km), we adopt a simple two isotropic layer structure, separated by an horizontal interface. This minimal parametrisation is able to reproduce the main feature, i.e. the strong positive pulse, on the Constant plot (see Fig. 4) without introducing any 3D complexity. Zone B1 (from $X=175$ to $X=205$ km) is parametrised using a four layer structure. The uppermost layer represents the Tyrrhenian crust as in Zone A, the mantle wedge is divided between the two middle layers, where the upper one is isotropic and the lower one is anisotropic. No velocity jump between the two is allowed. The lowermost layer shapes the subducted crust, separated from the mantle wedge by a seismic velocity discontinuity. This parametrisation introduces some 3D heterogeneities in the mantle wedge, leaving both the Tyrrhenian and the subducted crust isotropic. As described in the previous section, between $X=205$ and $X=225$ km (Zone B2), we identify an anisotropic zone at depth, cut by a positive seismic velocity jump (e.g. where seismic velocity increases with depth). To reproduce such complexity, we adopt a parametrisation composed of five layers. We do not identify a clear, well developed Tyrrhenian Moho, so we use a single isotropic layer to represent from the surface of the Apenninic wedge to the top of the anisotropic area. Here, we introduce two anisotropic layers. The upper one shares the same seismic velocity as the uppermost layer, while the lower one might have higher seismic velocities. These two layers represent the bottom of the wedge and the upper part of the subducting crust. An isotropic layer defines the rest of the subducting crust, separated by the underlying Adriatic mantle by a positive velocity jump. Zone B3 (from $X=225$ to $X=245$ km) displays simpler features with respect to Zone B2. Here,

anisotropy is confined in the entire subducting crust. A three layer parametrisation is adopted. The uppermost layer represents the Apenninic wedge; a second anisotropic layer is introduced at its bottom without a seismic velocity jump between the two layers. Finally a half-space represents the subducting Adriatic mantle. From $X = 245$ km to the Adriatic sea (Zone C), we identify a single seismic discontinuity, and we adopt here the same parametrisation as for the Tyrrhenian side.

In Figure 6 and Table S2, we report the result of the two-step inversion. The upper panel in Figure 6 shows the retrieved model for the seismic structure along profile AA'. Dashed lines indicate the positive seismic discontinuities at depth. The purple area is the anisotropic zone detected in our analysis, where the arrows report the directions of the symmetry axis of the anisotropic materials, projected along the profile. Numbers refer to the S -velocities used in the second step of the inversion, for each zone. Topography is reported on top for reference, together with the subdivision of the profile in three zones. The middle and lower panel in Figure 6 display the harmonic decomposition of the synthetic data-set computed using the model in the upper panel. Only Constant and N-S parts are reported, as low energy is present in the E-W plot. The comparison between the middle and lower panels in Figures 6 and 4, shows that the retrieved model reproduces fairly well the main features found in the harmonic decomposition of the RF data-set, which are the foci of this study. In particular, on the Constant plot, the signals associated to the Tyrrhenian and Adriatic Mohos, together with the P_s from the top of

the subducted plate, are correctly modeled both in their geometry and in their amplitudes. On the N-S plot, the anisotropic interfaces give rise to a combination of pulses which fairly resembles the observed harmonic decomposition. However, we note that our simple inversion scheme does not account for second-order features, such as the negative phase at about 80 km depth along the Adriatic coast, or the multiple phases from the Tyrrhenian Moho, which are likely to arrive at about 10 s (and migrate at 80–100 km depth) between $X = 30$ and $X = 180$ km along the profile).

The retrieved model gives a quantitative estimate to the proposed interpretation. Moving from the Adriatic side toward the Tyrrhenian side, we observe that Zone C is characterised by a west-dipping interface separating the Adriatic crust from the upper mantle. Such interface is sub-horizontal from $X = 320$ km to $X = 290$ km, at a depth about 40 km. At $X = 290$ km, the Adriatic Moho dips into the mantle to about 60 km. In Zone B3, the lower part of the Adriatic crust, transported between 45 and 65 km depth, exhibits an anisotropic behaviour, but does not show a first-order increase in the isotropic S -velocity ($V_s = 3.8$ km/s). Slow anisotropic axes display a coherent dipping direction, 15° , incident to the normal of the dipping Adriatic Moho. Zone B2 presents the highest degree of complexity for our study area. Here, the Adriatic Moho continues to dip, possibly increasing its dip angle, reaching about 80 km depth. Above it, a new S -velocity discontinuity appears almost parallel to the Adriatic Moho (i.e. west-dipping, from 50 to 60 km depth). This interface separates the subducted Adriatic lower crust from the wedge.

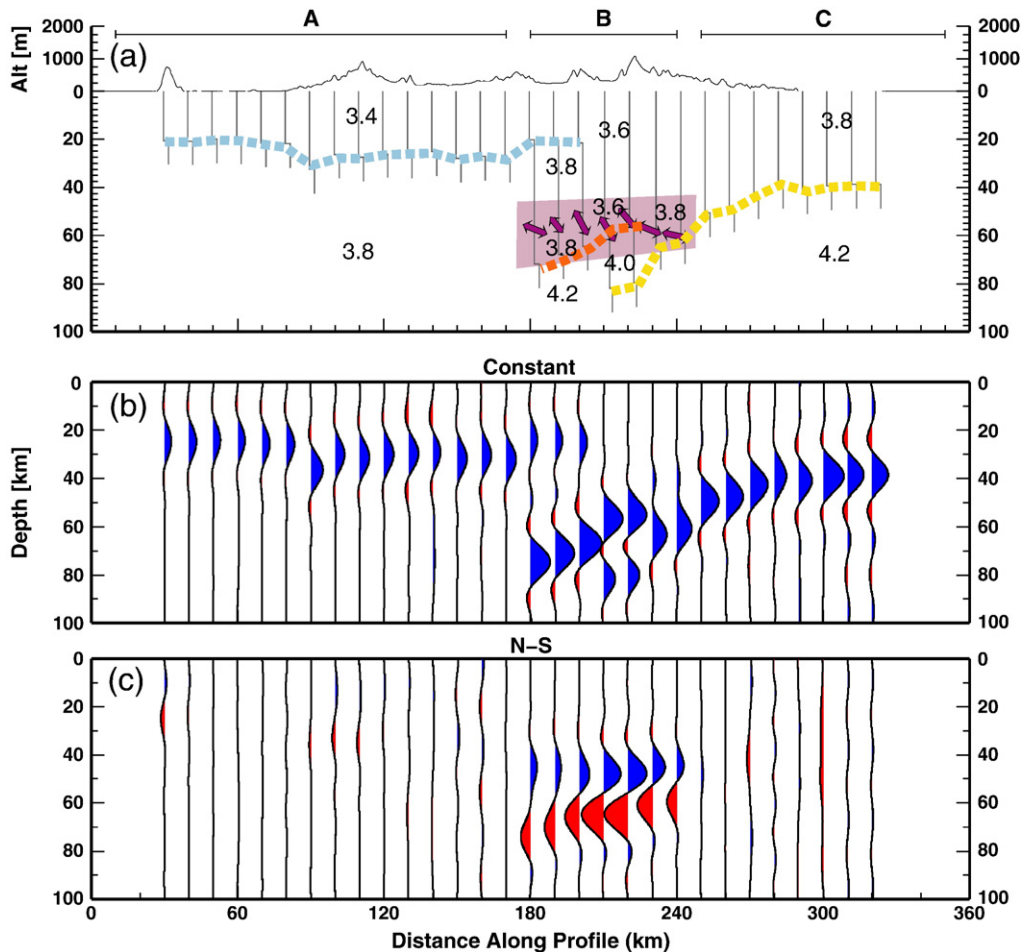


Fig. 6. (a) Seismic model of the study area (see Table S2, for details). Cyan, orange and yellow lines indicate the isotropic seismic discontinuities. Numbers report the S -wave velocity (in km/s). The purple area marks the depth level where anisotropy develops. Anisotropic symmetry axes (arrow) are projected on the profile section. Topography and profile subdivision are plotted on top. (b–c) Harmonic decomposition of the synthetic RF data-set obtained using the seismic model in (a): “constant” $k = 0$ term in (b); and N-S $\cos\phi$ term in (c).

S-velocity increases, with respect to Zone B1, in the subducted lower-crust to 4.0 km/s, while the wedge almost maintains the mean S-velocity of the Adriatic crust. Anisotropy is still confined between 45 and 65 km depth, but now it develops between the wedge and the subducted lower crust. Anisotropic axes are almost normal to the isotropic dipping interfaces. In Zone B1, the Tyrrhenian Moho appears as a shallow interface at about 20 km depth. The wedge is composed of an isotropic upper zone (20–25 km thick) and an anisotropic lower zone (25–30 km thick), above the subducted Adriatic lower crust. The upper interface of the subducted lower crust dips toward W, from 65 to 75 km depth. The Tyrrhenian crust is characterised by a low S-velocity (3.4 km/s). S-velocity increases in the wedge to 3.8 km/s. The subducted Adriatic lower crust displays a seismic S-velocity which equals the velocity in the Adriatic lithospheric mantle (about 4.2 km/s), so that its lower boundary results undefined. Anisotropy develops between 40 and 70 km depth, a slightly wider depth interval than in Zones B2 and B3. Anisotropic axes shift their directions, from almost normal to the subducted Adriatic crust (at about $X=220$ km) to a more horizontal trend (at about $X=180$ km). Finally, for Zone A (the Tyrrhenian side), the inversion confirms the presence of a sub-horizontal interface, separating a thin crust (20–30 km thick), characterised by low value of the mean S-velocity (3.4 km/s), from a low S-velocity upper mantle (3.8 km/s).

3.4. Interpretation

The inversion result gives a quantitative basis to our interpretation, both in term of interface depth and seismic velocity at depth. Here, we point out three key aspects of our results: the wedge, the subducted lower crust and the anisotropy. Focusing on the wedge, which develops in Zones B2 and B3, we observe that the S-velocity increases from E (3.6 km/s in Zone B2) toward W (3.8 km/s in Zone B1). At shallow depth, the wedge is composed of sediments and crustal slices off-scraped from the subducting plate (called crustal wedge or Apenninic wedge), while at larger depth sublithospheric upper mantle materials might be involved (indicated as wedge nose or mantle wedge, (Scrocca et al., 2007)). We do not identify a clear jump in the seismic properties of the wedge at depth, which might be a candidate for such transition (from crustal wedge to mantle wedge). This fact suggests a gradual transition between the two. Shifting our attention to the subducted lower crust, its seismic properties change following the same scheme as in the wedge (i.e. S-velocity increases from E toward W). However, S-velocity reaches higher values at relatively shallow depth (70–80 km depth). Considering a mean dip angle of about 30° , the thickness of the subducted lower crust ranges from 15 to 20 km.

A well defined anisotropic depth level is found under the orogen. Anisotropy starts to develop at about $X=240$ km and persists at least at about $X=180$ km. The minimum and maximum depths of the

anisotropy are almost constant along the profile, at about 45 and 65 km depth, respectively. The depth of the lower boundary slightly increases in its western termination, where the upper boundary seems to shallow. Anisotropic axes display an almost trench-normal orientation with coherent patterns in the different parts of the anisotropic zone. Anisotropy percentage is as high as about 7%, which reflects the presence of highly anisotropic materials (Hacker et al., 2003). Clearly, the anisotropy does not follow the isotropic structures previously illustrated (i.e. it is not trapped in the subducted lower crust nor develops exclusively in the mantle wedge). While the S-velocity evolution gives insights into the metamorphism of the subducted crustal materials, the evolution of the anisotropy seems to illuminate a different process related to the transformation of such materials, (R1.3) such as lattice preferred orientation (LPO) of olivine, or alignment of melt inclusions.

4. Discussion

Qualitative analysis of the harmonic decomposition of a large RF data-set along an anti-Apenninic profile, coupled with a global method for RF inversion, points out a number of new details of the seismic structure across the Apennines orogen, giving us a chance for supporting a regional scale interpretation of the geodynamic processes acting in the area. In Figure 7, we draw an interpretative sketch of the results obtained in this study. As briefly outlined at the end of Section 3.2, our analysis of the RF images points out: (1) the continental subduction of the Adriatic lower crust under the Northern Apennines at least down to 80 km depth; (2) the metamorphism and dehydration of such subducted Adriatic lower crust; (3) the migration of the fluids from the subducting plate toward the wedge. Results obtained using a global inversion scheme confirm these points.

4.1. Continental subduction

The retrieved geometry of the subsurface structures clearly mimics the presence of a subducted west-dipping layer under the Apennines crest. An almost flat, shallow Moho (about 25 km depth) characterises the Tuscan domain, while the Adriatic for-land displays a thicker crust (about 40 km thick). Our reconstruction confirms a first-order difference in the crustal structure at the two end-points of our profile that has been widely recognised (Piana Agostinetti and Amato, 2009). The “Tyrrhenian” shallow Moho can be observed along the profile from the coastal area to, at least, the most recent extensional basin, Val Tiberina basin, as previously observed in Piana Agostinetti et al. (2008a) for a neighbouring area. The Adriatic Moho is clearly visible its the easternmost portion of the profile, and readily starts to dip in the W direction. (R1.1) Mean V_s for the Tyrrhenian and Adriatic crusts are 3.4 and 3.8 km/s, respectively. This contrast reflects the different origins

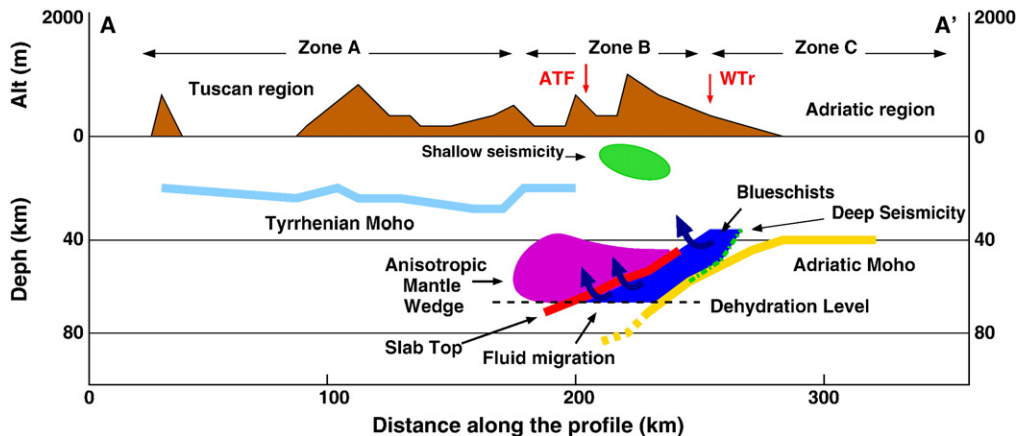


Fig. 7. Sketch for the proposed interpretation.

and compositions of the two crusts (Pauselli et al., 2010). Beneath the orogen, a new seismic interface develops parallel to the dipping Adriatic Moho, defining a low-velocity layer which plunges into the mantle. Such feature can be observed down to 80 km depth. From the continuity of the Adriatic Moho, we interpret it as a part of the Adriatic lower crust that is dragged downward with the Adriatic mantle lithosphere. Dip angle of such layer (about 30°) is consistent with worldwide observations of the dipping angle in the shallow part of subduction zones (Lallemand et al., 2005) and with the dip angle of the Wadati–Benioff plane (about 38°). The thickness of the subducted Adriatic lower crust is comprised between 15 and 20 km. This value is slightly larger than both the thickness found in Chiarabba et al. (2009) and the thickness which can cause subduction failure (Stern, 2002), as hypothesised in Faccenna et al. (2001). More, the evidence of widespread high pressure materials in the Tuscan domain (Brun and Faccenna, 2008) confirms that a large portion of Adriatic crust is dragged downward during the retreat of the subduction zone, possibly comprising slices of the upper crust (Wu et al., 2009). The amount of Adriatic crust impiled in the orogenic wedge is a still debated issue in the studies of the Apennines chain (e.g. Scrocca et al., 2005). Here, we find a thickness for the impiled materials of about 20–25 km, which implies that part of the basement is involved in the orogen. Such interpretation is in agreement with the hypothesis of the partial involvement of the magnetic basement in the orogenic wedge, as seen by magnetic data (Speranza and Chiappini, 2002). Also, this fact does well agree with the evidence of basement rocks found in a 5-km deep well in the area (S. Donato), consistent with a complete incorporation of the Adriatic upper crust in the orogenic wedge (Barchi et al., 1998).

4.2. Metamorphism and dehydration

Retrieved values of the seismic velocity V_s in the different parts of the low-velocity, dipping layer are consistent with the metamorphism of the subducted crust. The increase of the V_s in the subducted lower crust with depth reflects its progressive transformation (Kawakatsu and Watada, 2007). (R1.2) In this study, we suggest two main metamorphic phases. The first occurs at shallow depth (between 40 and 60 km), the other at about 65 km depth. Possible candidate materials for the phase transformations are: gabbro (or granulite) ($V_p \sim 3.9$ km/s at 1 GPa, Christensen (1996)) to blueschists ($V_s \sim 4.0$ km/s at 0.8 GPa, Fujimoto et al. (2007)), and blueschists to eclogite ($V_s > 4.4$ km/s, Christensen (1996)). Granulite, more than gabbro, can explain the low-level widespread seismicity which has been observed in the Adriatic lower crust (Piccinini et al., 2009). However, gabbro is likely to bear a larger amount of water (up to 5% H_2O , (Stern, 2002)) to depth, than a granulite. Eclogite is our preferred end-member for the lower crust metamorphism because it matches our observation due to its elevated seismic velocity and absence of anisotropy (Christensen and Mooney, 1995). At shallow depth, the subducted lower crustal rocks are changed to blueschists, which, in turn, are transformed in eclogite at larger depths (Stern, 2002). Blueschists display a strong anisotropic behaviour, with percentage as high as 5–10% (Fujimoto et al., 2007) and its transformation to eclogite release up to 2% H_2 (Hacker and Abers, 2004). The observation of anisotropy in the subducted crust suggests the formation of blueschists. Blueschists are a widely accepted candidate metamorphic faces for subduction metamorphism and has been postulated elsewhere (Helffrich, 2000). More, high pressure continental blueschists have been found in the Tuscan area, after the exhumation process active in the last 10–15 My (Jolivet et al., 1998).

4.3. Fluid migration in the mantle wedge

Fluid migration in the mantle wedge is testified by the development of anisotropy directly above the metamorphosed, subducted lower crust (Zones B1–B2). Water which enters the mantle wedge can induce either partial melting or serpentinization of peridotite. Serpentinization is often associated to mantle wedge materials where low seismic velocity,

high- V_p/V_s ratio are observed (e.g. Tibi et al., 2008). Serpentinized peridotite displays an anisotropic behaviour (Dewandel et al., 2003). Partial melting of the mantle wedge can produce diffuse microlensing which turns out to be highly anisotropic (Takei, 2010). The anisotropic zone of the mantle wedge found in this study can indicate a strong concentration of serpentine or partial melts. The absence of anisotropy under the Tuscan domain can reflect both the decrease of the concentration of the anisotropic materials and/or the breakup of the anisotropic pattern due to the asthenospheric mantle flow. The abrupt termination of the anisotropy at about 65 km depth beneath the Apennines, in coincidence with the disappearance of the low-velocity layer, defines a “dehydration level”. The low-velocity layer termination has been widely observed and associated to the complete transformation of the subducted lower crust to eclogite (Rondenay et al., 2008). Also, eclogite turns out to be almost isotropic (Christensen and Mooney, 1995). In our case, as suggested from the clear delimitation of the anisotropy at depth, the combination between the pressure–temperature conditions and the slow rate of subduction generates a clear level where all the blueschists are converted to eclogite and the water is released to the mantle wedge. The presence of such “dehydration level” has been hypothesised for the breakdown of amphiboles peridotite in oceanic subduction (Tatsumi and Eggins, 1995). The depicted scenario of fluid migration from the subducted crust to the mantle wedge can be combined with the long-standing observation of the retreat of the subducted plate (Malinverno and Ryan, 1986). If the “dehydration level” has been constant during the last ~10 My, the fluids escaped from the Adriatic crust did not concentrate in a single point of our profile (i.e. generating the classical “arc” magmatisms) but more likely hydrated all the Tyrrhenian uppermost mantle forming an hydrate mantle layer. This hypothesis is confirmed by the presence of diffuse attenuation in the upper portion of the Tyrrhenian mantle (Piccinini et al., 2010), widespread mantle layering found in the Tyrrhenian sea (Levin and Park, 2009) and the absence of clear arc magmatisms associated to the Northern Apennines subduction zone (Serri, 1997). The orientations of the anisotropic axes, which we retrieve in the different parts of the profile, are consistent with our hypothesis. Blueschists in the subducted lower crust display axes incident with the normal of the dipping interfaces. We argue that the stress field (i.e. simple shear) inside the subducted layer can induce allineation in the blueschist minerals (Fujimoto et al., 2007). In the hypothesis of partial melting, anisotropic axes in the mantle wedge can be aligned by the flow of the mantle materials which fill the gap due to the retreat of the plate. In this case, westernmost axes would be more horizontal, as observed (Takei, 2010).

Our interpretation of the fluid migration beneath the Apennines is likely to leave some evidence in the nature of the geochemical fluids reaching the surface in the orogen and the Tuscan region. Tuscany displays two main geothermal areas, Larderello and Mt. Amiata, and a variety of geothermal springs. Isotopic ratio He^3/He^4 contained in the spring water is a widely used marker to check its origin. A high He^3/He^4 ratio indicates that the fluids come from a mantle source and do not rest in the crust for a long time. On the contrary, a low value of the He^3/He^4 ratio would imply that the fluids come from a crustal source or they reside in the crust for a long time. Across the Northern Apennines, Minissale et al. (2000) found an increase of the He^3/He^4 ratio, from the orogen toward the Tuscan coast. This observation is in agreement with our interpretation, where the fluids, which do not transit through the mantle wedge, are released under the compressional front of the orogens, and (possibly) driven by the local fault system to the more recent extensional basin. Moving westward, fluids cross an increasing amount of mantle materials and the isotopic ratio increases. Near the Tuscan coast the ratio reaches its maximum value. Future investigations are needed to understand the diffusivity of such fluids through the upper Tuscan mantle.

It is worth to notice that the deeper seismicity is likely to be linked to the dehydration of the subducted Adriatic plate. Its linear trend displays a dip angle which is larger than the local dip of the subducted

crust. This phenomenon has been observed in other continental subductions (Ferris et al., 2003) and is related to the progressive dehydration of the subducted crust starting from its upper interface (Kirby et al., 2000). In its upper portion (between 35 and 50 km depth) the deeper seismicity shows a more concentrated behaviour and is confined to the subducted lower crust. Beneath 50 km depth the seismicity appears to be more diffuse around the subducted Adriatic Moho. This part of the seismicity might be related to the dehydration of the Adriatic mantle. Partial serpentinization of the margins of the Adria continental plate has been observed elsewhere (e.g. Beltrando et al. (2010)). In our setting, the subduction of the margins of the Adriatic plate can induce the release of water from serpentine in the uppermost part of the subducted lid, which in turn, can trigger earthquakes near the subducted Moho (Abers et al., 2009).

Finally, we observe that the main cluster of shallow seismicity is confined between the westernmost thrust and the easternmost extensional basin. This area sits directly above Zones B2 and B3, where we find evidence of the first metamorphic phase (gabbro to blueschists), where a large amount of water is released. We argue that these fluids are involved in the activation of the upper crust fault system. The importance of the uprising fluids for the local seismicity has been widely recognised (Chiarabba et al., 2009; Chiodini et al., 2004; Collettini et al., 2006). Here, we hypothesise that these fluids come from a deep crustal source related to the subduction of a slice of Adriatic crust.

5. Conclusion

In this study, we compute a large RF data-set from teleseismic waveforms recorded across the NAP orogen. The RF analysis and inversion highlight the details in the seismic structures buried under the chain and give new insight into the subduction process active in the area.

1. A first clear picture of the west-subducted Adriatic lower crust is depicted as it plunges in the upper mantle under this portion of the Northern Apennines (as a 15–20 km thick low *S*-velocity layer).
2. (R1.5) The *S*-velocity of the subducted Adriatic lower crust increases with depth, from 3.8 to 4.2 km/s. Seismic anisotropy develops in the 40–60 km depth range within the subducted crust. We suggest that such slice of lower crustal materials undergoes two main stage of metamorphism, during its dehydration process, from mafic granulite/gabbro to blueschists to eclogite;
3. Fluid migration from the subducted lower crust to the Apenninic wedge is recognised as the formation of a broad seismic anisotropic zone in the mantle wedge. As the subduction zone retreat, fluids diffusely hydrate the upper mantle beneath the Tuscan region.

More investigations are needed to understand how the depicted geodynamic scenario interacts with the intrinsic 3D morphology of the NAP orogen.

Supplementary materials related to this article can be found online at doi:10.1016/j.epsl.2010.10.039.

Acknowledgements

We thank Giovanni Chiodini for a fruitful discussion about geochemical fluids. We thank Claudio Faccenna and an anonymous reviewer for their constructive comments. Daniele Melini helped us in the computation on the INGV cluster. NPA thanks the Osservatorio Ximeniano di Firenze for logistical support. IB is supported by DPC-S1 URO2.02. NPA is supported by project Airplane (funded by the Italian Ministry of Research, Project RBPR05B2ZJ 003). Part of the data were recorded during RETREAT project (NSF grants EAR-0208652 and

EAR-0242291). Figures were drawn using GMT (Wessel and Smith, 1998).

References

- Abers, G., MacKenzie, L.S., Rondenay, S., Zhang, Z., Wech, A.G., Creager, K.C., 2009. Imaging the source region of Cascadia tremor and intermediate-depth earthquakes. *Geology* 37, 1119–1122. doi:10.1130/G30143A.1.
- Audet, P., Bostock, M.G., Christensen, N.I., Peacock, S.M., 2009. Seismic evidence for overpressured subducted oceanic crust and megathrust fault sealing. *Nature* 457, 76–78. doi:10.1038/nature07650.
- Bannister, S., Yu, J., Leitner, B., Kennett, B.L.N., 2004. Variations in crustal structure across the transition from West to East Antarctica, Southern Victoria Land. *Geophys. J. Int.* 155, 870–880.
- Barchi, M., Feyter, A.D., Magnani, M., Minelli, G., Pialli, G., Sotera, M., 1998. The structural style of the Umbria–Marche fold and thrust-belt. *Mem. Soc. Geol. It.* 52, 557–578.
- Beltrando, M., Rubatto, D., Manatschal, G., 2010. From passive margins to orogens: the link between ocean–continent transition zones and (ultra)high-pressure metamorphism. *Geology* 38, 559–562. doi:10.1130/G30768.1.
- Bianchi, I., Piana Agostinetti, N., De Gori, P., Chiarabba, C., 2008. Deep structure of the Colli Albani volcanic district (central Italy) from receiver functions analysis. *J. Geophys. Res.* 113, B09313. doi:10.1029/2007JB005548.
- Bianchi, I., Park, J., Piana Agostinetti, N., Levin, V., 2010. Mapping seismic anisotropy using harmonic decomposition of receiver functions: An application to Northern Apennines, Italy. *J. Geophys. Res.* 115, B12317 doi:10.1029/2009JB007061.
- Brudzinski, M.R., Thurber, C.H., Hacker, B.R., Engdahl, R., 2007. Global prevalence of double Benioff zones. *Science* 316, 1472–1474. doi:10.1126/science.1139204.
- Brun, J.P., Faccenna, C., 2008. Exhumation of high-pressure rocks driven by slab rollback. *Earth Planet. Sci. Lett.* 272, 1–7.
- Carminati, E., Wortel, M., Meijer, P., Sabadini, R., 1998. The two-stage opening of the western central Mediterranean basins: a forward modeling test to a new evolutionary model. *Earth Planet. Sci. Lett.* 160, 667–679.
- Channell, J.E.T., Mareschall, J.C., 1989. Alpine tectonics. Delamination and asymmetric lithospheric thickening in the development of the Tyrrhenian rift: Geological Society special Publication, 45, pp. 285–302.
- Chiarabba, C., De Gori, P., Speranza, F., 2009. Deep geometry and rheology of an orogenic wedge developing above a continental subduction zone: seismological evidence from the northern-central Apennines (Italy). *Lithosphere* 1, 95–104.
- Chiodini, G., Cardellini, C., Amato, A., Boschi, E., Caliro, S., Frondini, F., Ventura, G., 2004. Carbon dioxide Earth degassing and seismogenesis in central and southern Italy. *Geophys. Res. Lett.* 31. doi:10.1029/2004GL019480.
- Christensen, N.I., 1996. Poisson's ratio and crustal seismology. *J. Geophys. Res.* 101, 3139–3156.
- Christensen, N.I., Mooney, W.D., 1995. Seismic velocity structure and composition of the continental crust: a global view. *J. Geophys. Res.* 100, 9761–9788.
- Collettini, C., De Paola, N., Holdsworth, R.E., Barchi, M., 2006. The development and behaviour of low-angle normal faults during Cenozoic asymmetric extension in the Northern Apennines, Italy. *J. Struct. Geol.* 28, 333–352.
- De Luca, G., Cattaneo, M., Monachesi, G., Amato, A., 2009. Seismicity in central and northern Apennines integrating the Italian national and regional networks. *Tectonophysics*. doi:10.1016/j.tecto.2008.11.032.
- Dewandel, B., Boudier, F., Kern, H., Warsi, W., Mainprice, D., 2003. Seismic wave velocity and anisotropy of serpentinized peridotite in the Oman ophiolite. *Tectonophysics* 370, 77–94.
- Dewey, J.K., Helman, M.L., Hutton, D.H.W., Knot, S.D., 1989. Kinematics of the western Mediterranean. *Geol. Soc. Spec. Publ.* 45, 265–283.
- Di Stefano, R., Kissling, E., Chiarabba, C., Amato, A., Giardini, D., 2009. Shallow subduction beneath Italy: three-dimensional images of the Adriatic–European–Tyrrhenian lithosphere system based on high-quality P wave arrival times. *J. Geophys. Res.* doi:10.1029/2008JB005641.
- Faccenna, C., Becker, T.W., Lucente, F.P., Jolivet, L., Rossetti, F., 2001. History of subduction and back-arc extension in the Central Mediterranean. *Geophys. J. Int.* 145, 809–820.
- Ferris, A., Abers, G.A., Christensen, D.H., Veenstra, E., 2003. High resolution image of the subducted Pacific (?) plate beneath central Alaska. *Earth Planet. Sci. Lett.* 214, 575–588.
- Finetti, I. (Ed.), 2005. CROP Project: deep seismic exploration of the Central Mediterranean and Italy. *Atlases in Geoscience*, volume 1. Elsevier.
- Frederiksen, A.W., Bostock, M.G., 2000. Modeling teleseismic waves in dipping anisotropic structures. *Geophys. J. Int.* 141, 401–412.
- Frepoli, A., Amato, A., 1997. Contemporaneous extension and compression in the northern Apennines from earthquake fault-plane solutions. *Geophys. J. Int.* 129.
- Fujimoto, Y., Kono, Y., Ishikawa, M., Hirajima, T., Arima, M., 2007. Vp and Vs measurements of blueschists: implications for the origin of high-Poisson's ratio anomalies in the subducting slab. *Japan Geoscience Union*.
- Hacker, B., Abers, G., 2004. Subduction factory 3: an excel worksheet and macro for calculating the densities, seismic wave speeds, and H₂O contents of minerals and rocks at pressure and temperature. *Geochem. Geophys. Geosyst.* 5. doi:10.1029/2003GC000614.
- Hacker, B.R., Abers, G., Peacock, S., 2003. Subduction factory 1. Theoretical mineralogy, densities, seismic wave speeds, and H₂O contents. *J. Geophys. Res.* 108. doi:10.1029/2001JB001127.
- Helffrich, G., 2000. Subduction: top to bottom. *American Geophysical Union. Chapter Subducted lithospheric slab velocity structure: observations and mineralogical inferences*. Number 96 in *Geophysical monograph*, pp. 215–222.

- Iwamori, H., 1998. Transportation of H_2O and melting in subduction zones. *Earth Planet. Sci. Lett.* 160, 65–80.
- Jolivet, L., Faccenna, C., Rossetti, F., Storti, F., 1998. Midcrustal shear zones in postorogenic extension: example from the northern Tyrrhenian sea. *J. Geophys. Res.* 103, 12123–12161.
- Kawakatsu, H., Watada, S., 2007. Seismic evidence for deep-water transportation in the mantle. *Science* 306, 1468.
- Kirby, S., England, R.E., Denlinger, R., 2000. Subduction: top to bottom. American Geophysical Union. Chapter Intermediate- depth intraslab earthquakes and arc volcanism as physical expression of crustal and upper mantle metamorphism in subducting slab. Number 96 in Geophysical monograph, pp. 195–214.
- Lallemand, S., Heuret, A., Boutelier, D., 2005. On the relationships between slab dip, back-arc stress, upper plate absolute motion, and crustal nature in subduction zones. *Geochem. Geophys. Geosyst.* 6. doi:10.1029/2005GC000917.
- Langston, C.A., 1979. Structure under Mount Rainier, Washington, inferred from teleseismic body waves. *J. Geophys. Res.* 84, 4749–4762.
- Levin, V., Park, J., 1998. P-SH conversions in layered media with hexagonally symmetric anisotropy: a cookbook. *Pure Appl. Geophys.* 151, 669–697.
- Levin, V., Park, J., 2009. New constraints on the crustal structure beneath northern Tyrrhenian sea. *Eos Trans. AGU. Fall Meet. Suppl., Abstract, T44A-05.*
- Levin, V., Margheriti, L., Park, J., Amato, A., 2002. Anisotropic seismic structure of the lithosphere beneath the Adriatic coast of Italy constrained with mode-converted body waves. *Geophys. Res. Lett.* doi:10.1029/2002GL015438.
- Lucente, F.P., Chiarabba, C., Cimini, G.B., Giardini, D., 1999. Tomographic constraints on the geodynamic evolution of the Italian region. *J. Geophys. Res.* 104, 20307–20327.
- Lucente, F.P., Piana Agostinetti, N., Moro, M., Selvaggi, G., Di Bona, M., 2005. Possible fault plane in a seismic gap area of the Southern Apennines (Italy) revealed by receiver functions analysis. *J. Geophys. Res.* 110. doi:10.1029/2004JB003187.
- Malinverno, A., Ryan, W.B.F., 1986. Extension in the Tyrrhenian sea and shortening in the Apennines as results of arc migration driven by sinking of the lithosphere. *Tectonics* 5, 227–245.
- Mariucci, M.T., Amato, A., Montone, P., 1999. Recent tectonic evolution and present stress in the Northern Apennines (Italy). *Tectonics* 18, 108–118.
- Mele, G., Sandvol, E., 2003. Deep crustal roots beneath the Northern Apennines inferred from teleseismic receiver functions. *Earth Planet. Sci. Lett.* 211, 69–78.
- Mercier, J.P., Bostock, M.G., Audet, P., Gaherty, J.B., Garnero, E.J., Revenaugh, J., 2008. The teleseismic signature of fossil subduction: Northwestern Canada. *J. Geophys. Res.* 113. doi:10.1029/2007JB005127.
- Minissale, A., Magro, G., Martinelli, G., Vaselli, O., Tassi, G.F., 2000. Fluid geochemical transect in the Northern Apennines (central-northern Italy): fluid genesis and migration and tectonic implications. *Tectonophysics* 319, 199–222.
- Montone, P., Mariucci, M.T., Pondrelli, S., Amato, A., 2004. An improved stress map for Italy and surrounding regions (central Mediterranean). *J. Geophys. Res.* 109. doi:10.1029/2003JB00270.
- Park, J.J., Levin, V., 2000. Receiver functions from multiple-taper spectral correlation estimates. *Bull. Seismol. Soc. Am.* 90, 1507–1520.
- Park, J.J., Yuan, H., Levin, V., 2004. Subduction zone anisotropy beneath Corvallis, Oregon: a serpentinite skid mark of trench-parallel terrane migration? *J. Geophys. Res.* 109. doi:10.1029/2003JB002718.
- Patacca, E., Scandone, P., Di Luzio, E., Cavinato, G.P., Parotto, M., 2008. Structural architecture of the central Apennines: interpretation of the CROP 11 seismic profile from the Adriatic coast to the orographic divide. *Tectonics* 27, TC3006. doi:10.1029/2005TC001917.
- Pauselli, C., Federico, C., 2002. The brittle/ductile transition along the crop03 seismic profile: relationship with the geological feature. *Boll. Soc. Geol. It. Spec.* 1, 25–35.
- Pauselli, C., Ranalli, G., Federico, C., 2010. Rheology of the Northern Apennines: Lateral variations of lithospheric strength. *Tectonophysics* 484, 27–35. doi:10.1016/j.tecto.2009.08.029.
- Piana Agostinetti, N., Amato, A., 2009. Moho depth and v_p/v_s ratio in peninsular Italy from teleseismic receiver functions. *J. Geophys. Res.* 114, B06303. doi:10.1029/2008JB005899.
- Piana Agostinetti, N., Malinverno, A., 2010. Receiver function inversion by trans-dimensional Monte Carlo sampling. *Geophys. J. Int.* doi:10.1111/j.1365-246X.2010.04530.x.
- Piana Agostinetti, N., Lucente, F.P., Selvaggi, G., Di Bona, M., 2002. Crustal structure and Moho geometry beneath the Northern Apennines (Italy). *Geophys. Res. Lett.* 29. doi:10.1029/2002GL015109.
- Piana Agostinetti, N., Levin, V., Park, J., 2008a. Crustal structure above a retreating trench: receiver function study of the northern Apennines orogen. *Earth Planet. Sci. Lett.* 275, 211–220. doi:10.1016/j.epsl.2008.06.022.
- Piana Agostinetti, N., Park, J.J., Lucente, F.P., 2008b. Mantle wedge anisotropy in Southern Tyrrhenian subduction zone (Italy), from receiver function analysis. *Tectonophysics* 462, 35–48. doi:10.1016/j.tecto.2008.03.020.
- Piccinini, D., Piana Agostinetti, N., Roselli, P., Ibs-von Seht, M., Braun, T., 2009. Analysis of small magnitude seismic sequences along the Northern Apennines (Italy). *Tectonophysics* 476, 136–144. doi:10.1016/j.tecto.2009.04.005.
- Piccinini, D., Di Bona, M., Lucente, F.P., Levin, V., Park, J., 2010. Seismic attenuation and mantle wedge temperature in the northern Apennines subduction zone (Italy) from teleseismic body wave spectra. *J. Geophys. Res.* 115, B09309. doi:10.1029/2009JB007180.
- Pondrelli, S., Salimbeni, S., Ekstrom, G., Morelli, A., Gasperini, P., Vannucci, G., 2006. The Italian CMT dataset from 1977 to the present. *Physics of The Earth and Planetary Interiors* 159 (3–4), 286–303. doi:10.1016/j.pepi.2006.07.008.
- Reyners, M., Eberhart-Phillips, D., Stuart, G., Nishimura, Y., 2006. Imaging subduction from the trench to 300 km depth beneath the central North Island, New Zealand, with Vp and Vp/Vs. *Geophys. J. Int.* 165, 565–583.
- Rondenay, S., Abers, G.A., van Keken, P.E., 2008. Seismic imaging of subduction zone metamorphism. *Geology* 36, 275–278. doi:10.1130/G24112A.1.
- Roselli, P., Lucente, F.P., Piana Agostinetti, N., 2008. Crustal structure at colliding plates boundary from receiver functions analysis: a close look beneath the northern Apennines (Italy). *Geophys. Res. Lett.* 35. doi:10.1029/2008GL034055.
- Roselli, P., Piana Agostinetti, N., Braun, T., 2010. Shear-velocity and anisotropy structure of a retreating extensional forearc (Tuscany, Italy) from receiver functions inversion. *Geophysical Journal International* 181, 545–556. doi:10.1111/j.1365-246X.2010.04520.x.
- Sambridge, M., 1999. Geophysical inversion with a neighbourhood algorithm – I. Searching a parameter space. *Geophys. J. Int.* 138, 479–494.
- Savage, M., 1998. Lower crustal anisotropy or dipping boundaries? Effects on receiver functions and a case of study in New Zealand. *J. Geophys. Res.* 103, 69–87.
- Savage, M., Park, J., Todd, H., 2007. Velocity and anisotropy structure at the Hikurangi subduction margin, New Zealand from receiver functions. *Geophys. J. Int.* 168, 1034–1050.
- Scrocca, D., Carminati, E., Doglioni, C., 2005. Deep structure of the Southern Apennines (Italy): thin-skinned or thick-skinned? *Tectonics* 24, TC3005. doi:10.1029/2004TC001634.
- Scrocca, D., Carminati, E., Doglioni, C., Marcantoni, D., 2007. Slab retreat and active shortening along the central-northern Apennines. In: Lacombe, O., Lave', J., Roure, F., Verges, J. (Eds.), *Thrust Belt and Foreland Basins*. Springer. chapter 25.
- Selvaggi, G., Amato, A., 1992. Subcrustal earthquakes in the Northern Apennines (Italy): evidence for a still active subduction? *Geophys. Res. Lett.* 19, 2127–2130.
- Serri, G., 1997. Neogene-Quaternary magmatic activity and its geodynamic implication in the Central Mediterranean region. *Annals of Geophysics XL*, pp. 681–703.
- Shiomi, K., Park, J., 2008. Structural features of the subducting slab beneath the Kii Peninsula, central Japan: seismic evidence of slab segmentation, dehydration, and anisotropy. *J. Geophys. Res.* 113. doi:10.1029/2007JB005535.
- Speranza, F., Chiappini, M., 2002. Thick-skinned tectonics in the external Apennines, Italy: new evidence from magnetic anomaly analysis. *J. Geophys. Res.* 107, 2290. doi:10.1029/2000JB000027.
- Steckler, M.S., Piana Agostinetti, N., Wilson, C.K., Roselli, P., Seeber, L., Amato, A., Lerner Lam, A., 2008. Crustal structure in the southern Apennines from teleseismic receiver functions. *Geology* 36, 155–158.
- Stern, R.J., 2002. Subduction zones. *Rev. Geophys.* 40. doi:10.1029/2001RG000108.
- Takei, Y., 2010. Stress-induced anisotropy of partially molten rock analogue deformed under quasi-static loading test. *J. Geophys. Res.* 115. doi:10.1029/2009JB006568.
- Tatsumi, Y., Eggins, S., 1995. *Subduction Zone Magmatism*. Blackwell, Boston, MS.
- Tibi, R., Wiens, D.A., Yuan, X., 2008. Seismic evidence for widespread serpentinized forearc mantle along the Mariana convergence margin. *Geophys. Res. Lett.* 35. doi:10.1029/2008GL034163.
- Tonegawa, T., Hirahara, K., Shibutani, T., Iwamori, H., Kanamori, H., Shiomi, K., 2008. Water flow to the mantle transition zone inferred from a receiver function image of the Pacific slab. *Earth Planet. Sci. Lett.* 274, 346–354.
- Wessel, P., Smith, W.H.F., 1998. New, improved version of the generic mapping tools released. *EOS Trans. Am. Geophys. Union* 79, 579.
- Whitney, D.L., Teyssier, C., Rey, P.F., 2010. The consequences of crustal melting in continental subduction. *Lithosphere* 1, 323–327. doi:10.1130/L62.1.
- Wu, Y., Fei, Y., Jin, Z., Liu, X., 2009. The fate of subducted upper continental crust: an experimental study. *Earth Planet. Sci. Lett.* 282, 275–284.